LAWRENCE
LIVERMORE
NATIONAL
LABORATORY

LLNL-TR-722088

Structures and transitions in tungsten grain boundaries

T. Frolov, Q. Zhu, J. Marian, R. E. Rudd

February 7, 2017

Disclaimer

This work performed under the auspices of the U.S. Department of Energy by Lawrence Livermore National Laboratory under Contract DE-AC52-07NA27344.

Structures and transitions in tungsten grain boundaries

Timofey Frolov, Qiang Zhu, Jaime Marian and Robert E. Rudd

February 6, 2017

Objective

The objective of this study is to develop a computational methodology to predict structure, energies of tungsten grain boundaries as a function of misorientation and inclination. The energies and the mobilities are the necessary input for thermomechanical model of recrystallization of tungsten for magnetic fusion applications being developed by the Marian Group at UCLA.

Summary

Recrystallization determines the upper extent of the operating temperature of tungsten as a diverter or first-wall material. At temperatures above the onset of recrystallization, migrating grain boundaries sweep out defects that contribute to hardening. These processes make the recrystallized material unsuitable because of its brittleness. Thermomechanical models to predict recrystallization and its effect on mechanical properties have to be informed of the mechanisms of grain boundary migration their structure and kinetic properties at tokamak operating temperatures. In this work grain boundary structures and energies as a function of misorientation and inclination were generated using atomistic simulations. We examined several interatomic potentials available in the literature and benchmarked them against existing the DFT calculations. We find that different interatomic potentials predict very different values for the magnitude and anisotropy of the GB energy. Our calculations identify the potentials that give the best agreement with the DFT calculations. We also demonstrate that for most [110] symmetrical tilt boundaries studied the standard approach of constructing grain boundaries used in all previous calculations including DFT does not find the ground state at 0K and at finite temperature relevant to tokamak operation. We find new ground states of previously studied boundaries by performing grand canonical optimization of the structure. These grain boundary structures are characterized by high configurational complexity, which probably contributes to their stability at high temperature. The multiplicity of states suggests that grain boundaries in W exhibit phase behavior similar to Cu grain boundaries investigated in our previous work. The finding of the true ground states of grain boundaries has important consequences studies of recrystallization and embrittlement.

Background

Tungsten has been identified as the diverter material in ITER and is a leading candidate for the plasma-facing components in DEMO and subsequent magnetic fusion energy systems because of its high mechanical strength, high thermal conductivity, high melting point and low yield for sputtering by hydrogen isotopes. While tungsten has a number of favorable properties it is also intrinsically brittle even at relatively high temperatures especially after recrystallization. As materials are subjected to harsh conditions, their microstructure changes leading to changes in materials properties. The need to understand materials under these conditions motivates the development of computational models and simulations that can predict mechanical and kinetic properties of tungsten grain boundaries. Accumulating computational studies demonstrate that finding the ground state of grain boundaries is a challenging task that requires advanced grand canonical sampling[1, 2, 3, 4, 5, 6]. In addition recent experimental and computational studies demonstrated that elevated temperatures and changes in chemical composition could lead to structural transformations at grain boundaries that result in discontinuous changes in materials properties[7, 8, 9, 10, 11, 12]. Experimental studies linked these transitions to abnormal grain growth and embrittlement in metallic and ceramic systems[13, 14, 15]. We use atomistic simulations to predict grain boundary structures and structural transitions and investigate their effect on embrittlement and mobility in the context of recrystallization.

PROGRESS AND STATUS

Methods

Tungsten grain boundaries were modeled using four different potentials, three of which are the embedded-atom method (EAM) potentials EAM1[16], EAM2[17], EAM3[18, 19] and one is the bond-order potential (BOP)[20]. The predictions of the different models were benchmarked against the existing DFT calculations[21, 22]. Grain boundary structure and energy calculations were performed for two different sets of grain boundaries. The first set contained 246 [001] tilt boundaries with misorientation angle θ ranging from 0 to $\pi/2$ degrees and the inclination angle ϕ ranging from $-\pi/4$ to $\pi/4$ degrees. While the distinct grain boundary structures can be found within angular domain $0 < \theta < \pi/4$ and $0 < \phi < \pi/4$, we simulated grain boundary structures in the extended domain for future mobility calculations. The boundaries were obtained by rotating upper and lower grains around the common [001] axis by the angles $\theta/2$ and $-\theta/2$, respectively and then rotating each grain by the same angle ϕ. Figure 1a illustrates (θ, ϕ) map describing the misorientation and inclination angels of the grain boundaries studied in the work. The boundaries were chosen such as to minimize the grain boundary area for the computational efficiency, while evenly covering the entire angle range so that the spacing between the neighboring points is not larger than five degrees. On the plot the data points with $\phi = 0$ represent symmetrical tilt boundaries. All other boundaries are asymmetrical.

The second set contained fifty seven [110] symmetrical tilt boundaries, with the misorientation angle ranging from 0 to π. This set of boundaries was generated to compare grain boundary structures and energies to the results of previous DFT calculations[21, 22]. Grain

boundary structures and energies were calculated using the γ surface approach as well as by grand canonical sampling (GCS) technique.

The γ surface approach is a common method of constructing grain boundaries. In this approach two misoriented crystals are shifted relative to each other by a certain translation vector parallel to the future grain boundary plane. The translation is followed by a local relaxation of atoms that minimizes the energy of the system. Periodic boundary conditions are applied in the direction parallel to the boundary. This approach produces several different metastable states corresponding to different translation vectors. The configuration with the lowest grain boundary energy is assumed to be the ground state. It has been recognized that the γ surface method may not always find the ground state configuration. The first limitation is a lack of sampling: during the energy minimization atoms in the grain boundary region simply fall into the local energy minima, which means that other possible grain boundary configurations are not observed. The second limitation is that the sampling needs to be grand canonical: otherwise, the constant number of atoms in the system and periodic boundary conditions impose an unphysical constraint on possible grain boundary configurations. Despite these limitations the γ surface approach often yields ground states, it is computationally efficient and remains the standard method of grain boundary construction.

To validate the ground states predicted by the γ surface method we performed a full grand canonical sampling on a subset of boundaries at 0K. Motivated by recent studies on grain boundary phase transitions in Cu we selected $\Sigma5(310)[001]$ and $\Sigma5(210)[001]$ which are the typical high-angle high-energy boundaries with misorientation angles of 36.87 and 53.13 degrees, respectively. We also selected six [110] symmetrical tilt boundaries: $\Sigma33(118)[1\bar{1}0]$ (20.1°), $\Sigma19(116)[1\bar{1}0]$ (26.5°), $\Sigma3(112)[1\bar{1}0]$ (70.5°), $\Sigma(111)[1\bar{1}0]$ (109.5°), $\Sigma3(332)[1\bar{1}0]$ (129.5°) and $\Sigma27(552)[1\bar{1}0]$ (148.4°). These boundaries sample the entire misorientation range and have been investigated recently by DFT calculations. The GCS calculations are more computationally demanding compared to the simple γ surface approach, so the calculations were performed using only two out of four model potentials that we studied. The choice of potentials from Refs. [17, 16] was motivated by their better agreement with the DFT calculations[21, 22].

To validate the ground state structures calculated at 0K, we performed molecular dynamic simulations at high temperatures with grain boundaries terminated at open surfaces following the methodology proposed in Ref. [11]. A surface provides a source and sink for atoms and effectively introduces grand canonical environment in the grain boundary region. The simulations were performed in the temperature range from 1000K to 3000K. The initial states for the high temperature anneal where taken from both the γ surface construction as well as the CGS calculations to ensure that the final grain boundary state is independent of the initial conditions.

Grain boundary structures and energies from the γ surface approach

[100] tilt boundaries

The grain boundary energy of 246 [100]-tilt boundaries covering the entire misorientation and inclination range was calculated using four different potentials. The energy surface has several deep cusps. Figure 1 illustrates GB energy as a function of misorientation and

inclination for angles $\phi = 0°$, $\theta = 36.87°$ and $\theta = 53.13°$, respectively. Figure 1 illustrates grain boundary energy of symmetrical tilt boundaries as a function of misorientation. The two deep energy cusps on the plot correspond to $\Sigma5(310)[001]$ and $\Sigma5(210)[001]$ boundaries. The structure of these boundaries illustrated in Figure 2 is well known and composed of kite-shaped structural units. The left hand side panel of the figure shows grain boundary structure with the tilt axis normal to plane of the figure, while in the right hand side panel the tilt axis is parallel to the plane of the figure. While all four potentials predicts similar shape of the energy curve, the magnitude of the grain boundary energy shows significant difference. The EAM1 potential due to Marinica et al from Ref. [16] shows an excellent agreement with the DFT calculations of $\Sigma5(210)[001]$ boundary from Refs [21, 22]. These two boundaries are also energy cusps as a function of inclination as illustrated in Figures 1 c) and d). In addition to the difference in the magnitude of grain boundary energy , EAM1 and EAM2 potentials predict noticeably stronger anisotropy with changing inclination compared to the EAM3 and BOP potentials. Vicinal boundaries are expected to form steps as a result of the strong anisotropy, while more isotropic models predict homogeneous grain boundary structures. The presence of deep grain boundary energy cusps has consequences for grain boundary motion because vicinal boundaries may move by flow of steps. Therefore, the mobility of such boundaries is controlled by the mobility of steps.

Figure 1d) indicates for a given misorientation that the low energy configurations correspond to inclinations of $\phi = 0°$ and $\phi \sim \pm 45°$. The strong inclination anisotropy suggests that the boundaries with the intermediate inclinations should form facets composed of $\Sigma5(310)[001]$ and $\Sigma5(210)[001]$ symmetrical tilt boundaries. This faceting has been observed in bcc Fe by electron microscopy and molecular dynamic simulations[23]. Faceting has strong influence on grain boundary mobility as well. Increasing temperature is expected to decrease the grain boundary anisotropy, so the faceting may disappear as the melting temperature is approached. The exact temperature at which the defaceting occurs has to be determined from separate atomistic simulations.

[110] Symmetrical tilt boundaries

The magnitude of the grain boundary energy and the inclination anisotropy determines the driving force for coarsening and the mechanism of grain boundary motion which in turn influences the mobility. Since the different potentials studied here demonstrated very different predictions for both the magnitude and the degree of anisotropy, these predictions have to be checked against the existing DFT calculations. For this comparison we calculated grain boundary energies for the second set of [110] symmetrical tilt boundaries for which grain boundary energy was calculated for a large misorientation range using first principles methods[21, 22].

Figure 2 illustrates grain boundary energy as a function of misorientation calculated for [110] symmetrical tilt boundaries calculated using four different interatomic potentials. The plot also contains the DFT data from Refs. [21, 22]. The energies of the fifty seven boundaries were obtained using the γ-surface approach. It is evident from the figure that the different potentials predict similar trends, but provide significantly different magnitudes of the grain boundary energies. The grain boundary energy function has two deep cusps at 70.5° and 129.5° misorientation angles. The deepest energy cusp corresponds to $\Sigma3(112)[1\bar{1}0]$

boundary. The structure of this boundary is illustrated in Figure 3c).

Despite the similarity of the functional form of the energy curves predicted by the different potentials using the γ-surface approach, in some cases the different potentials predict very different grain boundary structures for the same misorientation angle. For example Figure 7a) and b) illustrates two different structures of the $\Sigma 33(118)[1\bar{1}0]$ (20.1°) boundary predicted by EAM1 and EAM2 potentials, respectively. The EAM1 structure agrees with the DFT calculations. At the same time EAM1 overestimates and EAM2 underestimates the DFT value by about the same amount. While EAM1 perfectly matches the grain boundary energy values for some boundaries, the EAM2 performs better on average for a number of [110] symmetrical tilt boundaries. These discrepancies motivate us to check whether the γ surface approach actually finds the ground states.

Grand Canonical Sampling (GCS) of grain boundary structure

We performed the grand canonical search for a subset of eight grain boundaries taken from a wide range of misorientation angles. In GCS approach, in addition to the rigid translations of the grains relative to each other, we change the atomic density at the boundary and sample different structures by displacing atoms in the grain boundary region from their ideal lattice positions. The calculations demonstrated that GCS yields the same ground states as the γ - surface approach for $\Sigma 5(210)[001]$, $\Sigma 5(310)[001]$, $\Sigma 3(112)[1\bar{1}0]$ and $\Sigma(111)[1\bar{1}0]$ boundaries. These boundaries correspond to energy cusps for [100] and [110] symmetrical tilt boundaries. Although atomically ordered states with higher atomic grain boundary density were observed upon loading of interstitials into $\Sigma 5(210)[001]$ grain boundary in bcc Mo [24], the energy of those states were found to be much higher than the energy of the ground state. The $\Sigma 3(112)[1\bar{1}0]$ boundary is very ordered and is the deepest energy cusp, so perhaps it is not surprising that is was found to be the ground state.

On the other hand, GCS applied to other four [110] boundaries yielded structures that were significantly different from the γ-surface generated configurations. These boundaries were selected to cover a wide range of misorientations away from the energy cusps located at 70.5° and 129.5°.

In the range $0° < \theta < 70.5°$ we selected the 20.1° and 26.5° misorientations. As discussed earlier, the γ surface approach configurations generated using EAM1 and EAM2 potentials are illustrated in Figure 7 a) and b), respectively. At an extra atomic fraction of 1/3 of the [118] plane, GCS predicts different grain boundary configurations with energies $\gamma_{GB} = 2.615$ J/m^2 and $\gamma_{GB} = 2.226$ J/m^2 for EAM1 and EAM2 potentials, respectively. These values are nearly degenerate with ones generated by the γ surface approach which yields $\gamma_{GB} = 2.611$ J/m^2 and $\gamma_{GB} = 2.257$ J/m^2 for these two potentials. The GCS generated structures are illustrated in Figure 7 c) and d). The GCS configurations are 1×3 reconstructions, which means that they have larger area compare to the γ - surface constructed boundary. Differently from the configuration in Figure 7a) and b), grain boundary atoms occupy positions between the [110] planes, while the planes of the two different grains are still aligned. This arrangement is analogous to structures of high temperature grain boundary phases found in previous work in Cu[7]. While the γ surface approach yields very different structures for EAM1 and EAM2, the GCS states are still not identical but remarkably similar. In fact GCS predicts a large number of grain boundary configurations of the type illustrated in Figure

7 c) and d) with nearly identical energies but slightly different arrangement of atoms along the tilt axis. This multiplicity of structures may contribute to the configurational entropy making these structures favorable at finite temperature.

In the angle range $129.5 < \theta < 180°$ we examined the $\Sigma27(552)[1\bar{1}0]$ boundary with a misorientation angle of 148°. Figure 4 illustrates multiple structures of of this grain boundary predicted by EAM2 potential. Figure 4a) shows the best configuration predicted by the traditional approach of γ-surface construction with GB energy $\gamma_{GB} = 2.67$ J/m^2, while b) and c) correspond to grain boundary structures obtained by GCS with atomic fractions 0 and 0.5 and energies $\gamma_{GB} = 2.495$ J/m^2 and $\gamma_{GB} = 2.493$ J/m^2, respectively. Notice that the configuration in Figure 4b) has much lower energy even though no atoms are added or removed from the grain boundary core just like in the γ surface approach. This example emphasizes the importance of sampling. Similar to the 20.5 and 26 boundaries discussed earlier, the GCS configurations of this boundary are 1×3 reconstructions with the grain boundary atoms also occupying positions between the [110] planes.

The GCS for other two boundaries with misorientations of 26.5° and 109.5° degrees demonstrated similar trends.

High temperature simulations

To validate the grain boundary structures generated at 0K by the GCS approach we annealed the bicrystals at high temperature following the simulation methodology proposed in our previous work[11]. In this approach instead of using periodic boundary conditions a grain boundary is terminated at an open surface. The surface acts as source and sink of atoms. During the simulation the atomic density of the boundary can adjust by the diffusion of atoms to and from the surface. The transport of atoms along the grain boundary is limited by diffusion, as a result, the system has to be annealed at a relatively high temperatures for tens of nanoseconds. To make sure that the final grain boundary structure is independent of the initial configuration we performed simulations with the initial structure taken from both γ-surface approach and GSC calculations.

Isothermal anneals of the $\Sigma5(310)[001]$ with an open surfaces confirmed that the 0K calculated structure was also stable at high temperature. To observe the metastable states with higher atomic density, we introduced interstitials into the bulk lattice just above the grain boundary plane and annealed the simulation blocks at 2000K and 2500K. In these simulations periodic boundary conditions were applied parallel to the grain boundary plane to eliminate sinks for the interstitial atoms. At both temperatures we first observed a formation of an ordered grain boundary structure that absorbed the interstitials. Figure 6b) illustrates the two different states of the boundary, which are similar to structures observed by Novoselov and Yunilkin in Mo[24]. This new metastable configuration exists for almost 100ns at 2000K and tens of nanoseconds at 2500K before it transforms into an interstitial loop at the boundary. The final stale of the boundary is illustrated in Figure 6b). The grain boundary segment confined between the two grain boundary dislocations is composed of perfect kite shaped structural units. These units appeared out of the metastable configuration with interstitials demonstrating that the kite structure of this boundary is very stable. The relatively long life of the metastable high energy state is probably due to a large barrier of transformation that involves nucleation of the dislocations. The energy analysis at 0K and

the simulations at high temperature demonstrate that the γ-surface approach predicts the ground state for these boundaries.

Very different behavior, but consistent with the 0K calculations, was found for the [110] boundaries. Figure 8 illustrates the bicrystal with the $\Sigma 27(552)[1\bar{1}0]$ grain boundary modeled with EAM1 potential that was annealed at 2500 K for 100 ns. The initial configuration was taken from the γ-surface approach. After the anneal the structure of the grain boundary is ordered and uniform throughout the bicrystal. Figure 8b) and c) illustrate the closer views of the structure with the tilt axis normal and parallel to the plane of the figure, respectively. Notice that the atoms in the grain boundary region occupy space in between the [110] atomic planes. The grain boundary structure matches the configuration obtained using GSC illustrated in figure 4c). This grain boundary structure has 50% extra atoms as a fraction of the (552) plane relative to the initial configuration obtained using the γ -surface approach, which means that the extra atoms diffused inside the grain boundary from the open surface during the simulation. In addition to changes in the grain boundary structure, the surface triple junction on the left-hand side of the figure shows a chevron reconstruction. Similar reconstructions were previously observed experimentally electron microscopy in Au[25, 26]. The atoms inside the triangular region have bcc structure. The two boundaries that form the chevron are the $\Sigma 3(112)[1\bar{1}0]$ (70.5) boundaries. Notice that the other surface triple junction does not undergo a similar reconstruction.

For the majority of the [110] symmetrical tilt boundaries with the exception of the two structures that correspond to energy cusps, the γ- surface approach is insufficient to predict grain boundary configurations at 0K and finite temperatures. On the other hand the GCS calculations predict new grain boundary ground states at 0K that remain to be the stable configurations at high temperature.

Acknowledgments

This work was performed under the auspices of the U.S. Department of Energy by Lawrence Livermore National Laboratory under Contract No. DE-AC52-07NA27344. We acknowledge the use of LC computing resources.

References

[1] S. R. Phillpot and J. M. Rickman, The Journal of Chemical Physics **97**, 2651 (1992).

[2] S. R. Phillpot, Phys. Rev. B **49**, 7639 (1994).

[3] S. von Alfthan, P. D. Haynes, K. Kashi, and A. P. Sutton, Phys. Rev. Lett. **96**, 055505 (2006).

[4] S. von Alfthan, K. Kaski, and A. P. Sutton, Phys. Rev. B **76**, 245317 (2007).

[5] A. L. S. Chua, N. A. Benedek, L. Chen, M. W. Finnis, and A. P. Sutton, Nat Mater **9**, 418 (2010).

[6] J. Zhang, C.-Z. Wang, and K.-M. Ho, Phys. Rev. B **80**, 174102 (2009).

[7] T. Frolov, M. Asta, and Y. Mishin, Current Opinion in Solid State and Materials Science , (2016).

[8] P. R. Cantwell, M. Tang, S. J. Dillon, J. Luo, G. S. Rohrer, and M. P. Harmer, Acta Materialia **62**, 1 (2014).

[9] T. Frolov, M. Asta, and Y. Mishin, Phys. Rev. B **92**, 020103 (2015).

[10] T. Frolov, S. V. Divinski, M. Asta, and Y. Mishin, Phys. Rev. Lett. **110**, 255502 (2013).

[11] T. Frolov, D. L. Olmsted, M. Asta, and Y. Mishin, Nat. Commun. **4**, 1899 (2013).

[12] T. Frolov, Applied Physics Letters **104**, (2014).

[13] S. J. Dillon and M. P. Harmer, Acta Materialia **55**, 5247 (2007).

[14] J. Luo, H. Wang, and Y.-M. Chiang, Journal of the American Ceramic Society **82**, 916 (1999).

[15] J. Luo, H. Cheng, K. M. Asl, C. J. Kiely, and M. P. Harmer, Science **333**, 1730 (2011).

[16] M. C. Marinica, L. Ventelon, M. R. Gilbert, L. Proville, S. L. Dudarev, J. Marian, G. Bencteux, and F. Willaime, Journal of Physics: Condensed Matter **25**, 395502 (2013).

[17] X. Zhou, H. Wadley, R. Johnson, D. Larson, N. Tabat, A. Cerezo, A. Petford-Long, G. Smith, P. Clifton, R. Martens, and T. Kelly, Acta Materialia **49**, 4005 (2001).

[18] G. J. Ackland and R. Thetford, Philosophical Magazine A **56**, 15 (1987).

[19] N. Juslin and B. Wirth, Journal of Nuclear Materials **432**, 61 (2013).

[20] N. Juslin, P. Erhart, P. Traskelin, J. Nord, K. O. E. Henriksson, K. Nordlund, E. Salonen, and K. Albe, Journal of Applied Physics **98**, 123520 (2005).

[21] W. Setyawan and R. J. Kurtz, Journal of Physics: Condensed Matter **26**, 135004 (2014).

[22] D. Scheiber, R. Pippan, P. Puschnig, and L. Romaner, Modelling and Simulation in Materials Science and Engineering **24**, 035013 (2016).

[23] D. Medlin, K. Hattar, J. Zimmerman, F. Abdeljawad, and S. Foiles, Acta Materialia **124**, 383 (2017).

[24] I. Novoselov and A. Yanilkin, Computational Materials Science **112, Part A**, 276 (2016).

[25] F. Lançon, T. Radetic, and U. Dahmen, Phys. Rev. B **69**, 172102 (2004).

[26] T. Radetic, F. Lançon, and U. Dahmen, Phys. Rev. Lett. **89**, 085502 (2002).

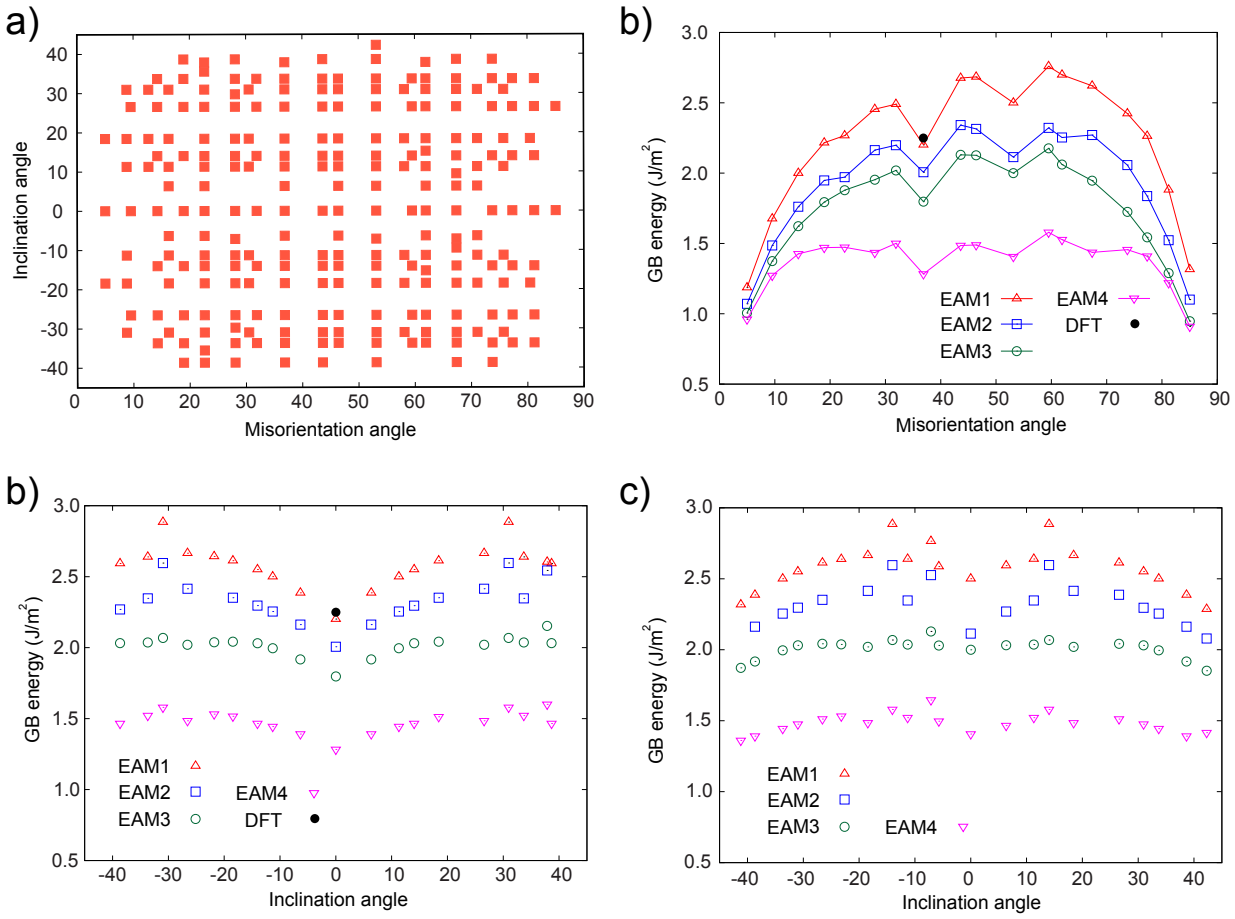

Figure 1: a)Studied 246 [001] tilt boundaries with misorientation angle ranging from 0 to 90 degrees and the inclination angle ranging from -45 to 45 degrees. b) Energy of symmetrical tilt boundaries calculated using four different potentials using γ -surface construction. Energy of $\Sigma5(310)[001]$ calculated with DFT. c) and d) GB energies as functions of inclination angle for misorientations of 36 and 53.13 degrees. Zero inclinations represent $\Sigma5(310)[001]$ and $\Sigma5(210)[001]$ symmetrical tilt boundaries, respectively.

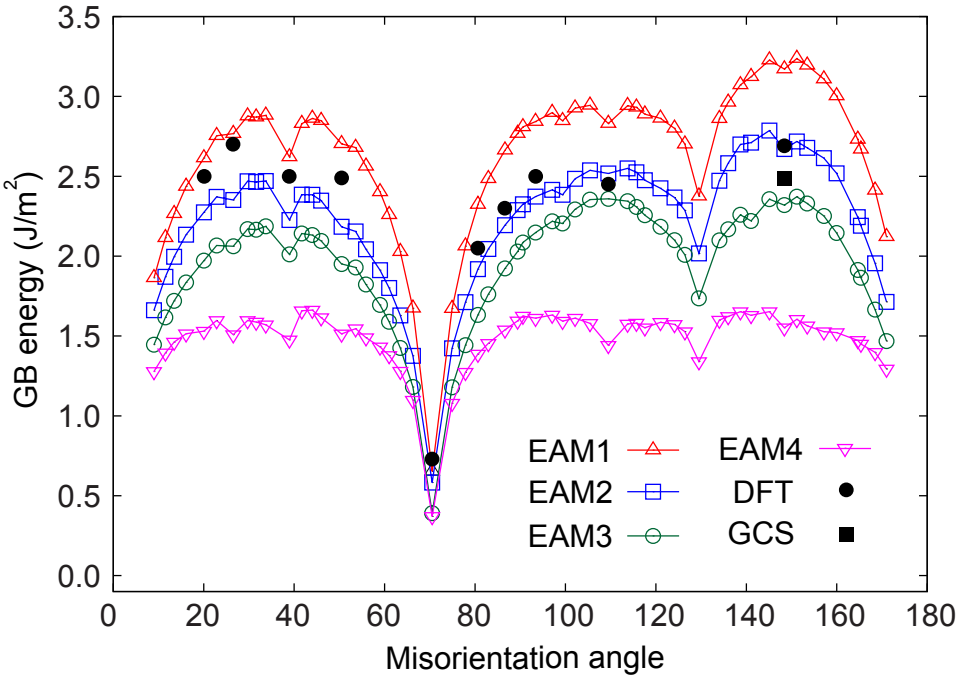

Figure 2: GB energy as a function of misorientation angle for [110] symmetrical tilt boundaries.

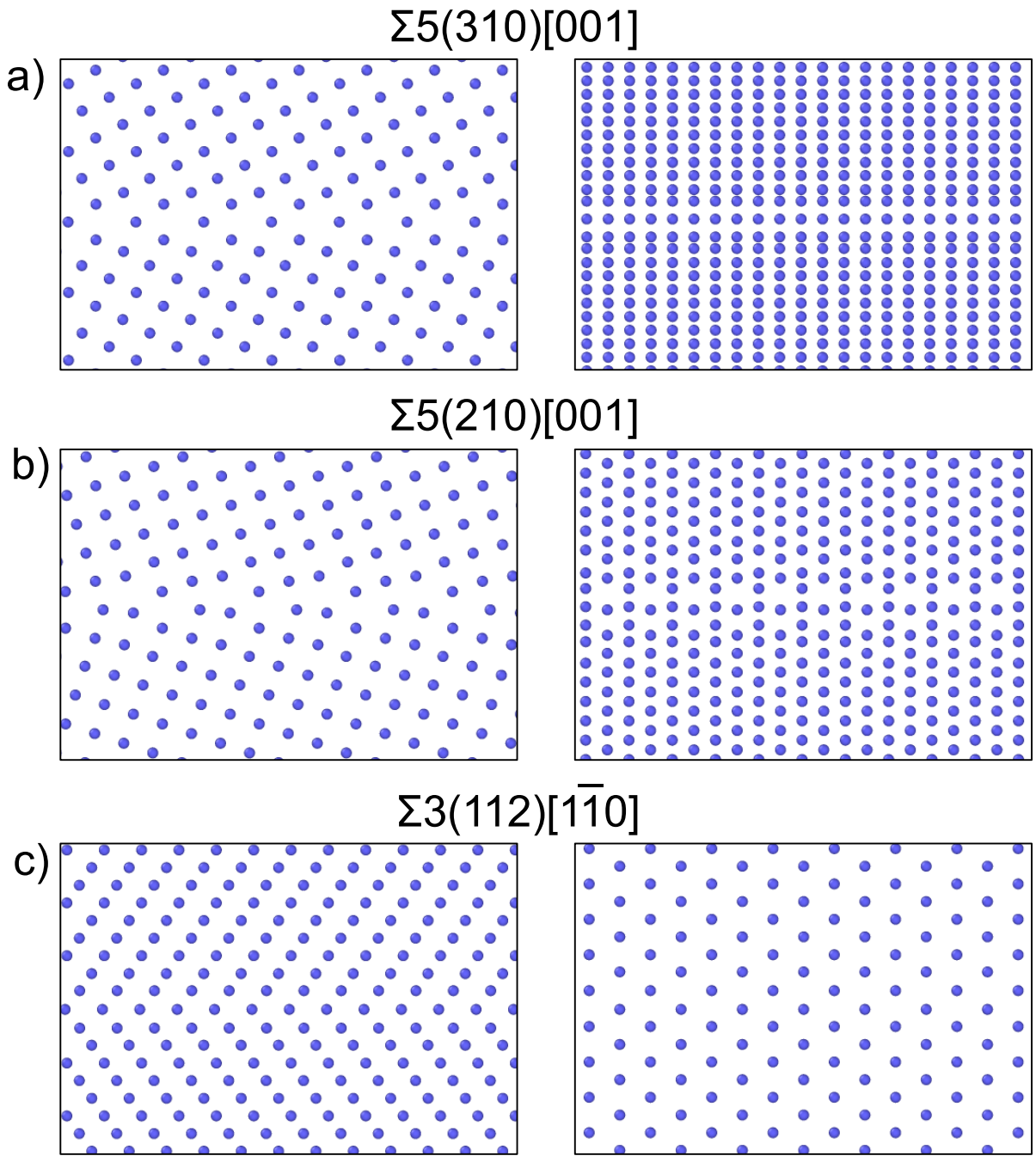

Figure 3: Examples of ground states of high angle [001] and [110]symmetrical tilt boundaries obtained by γ-surface construction and GCS methods.

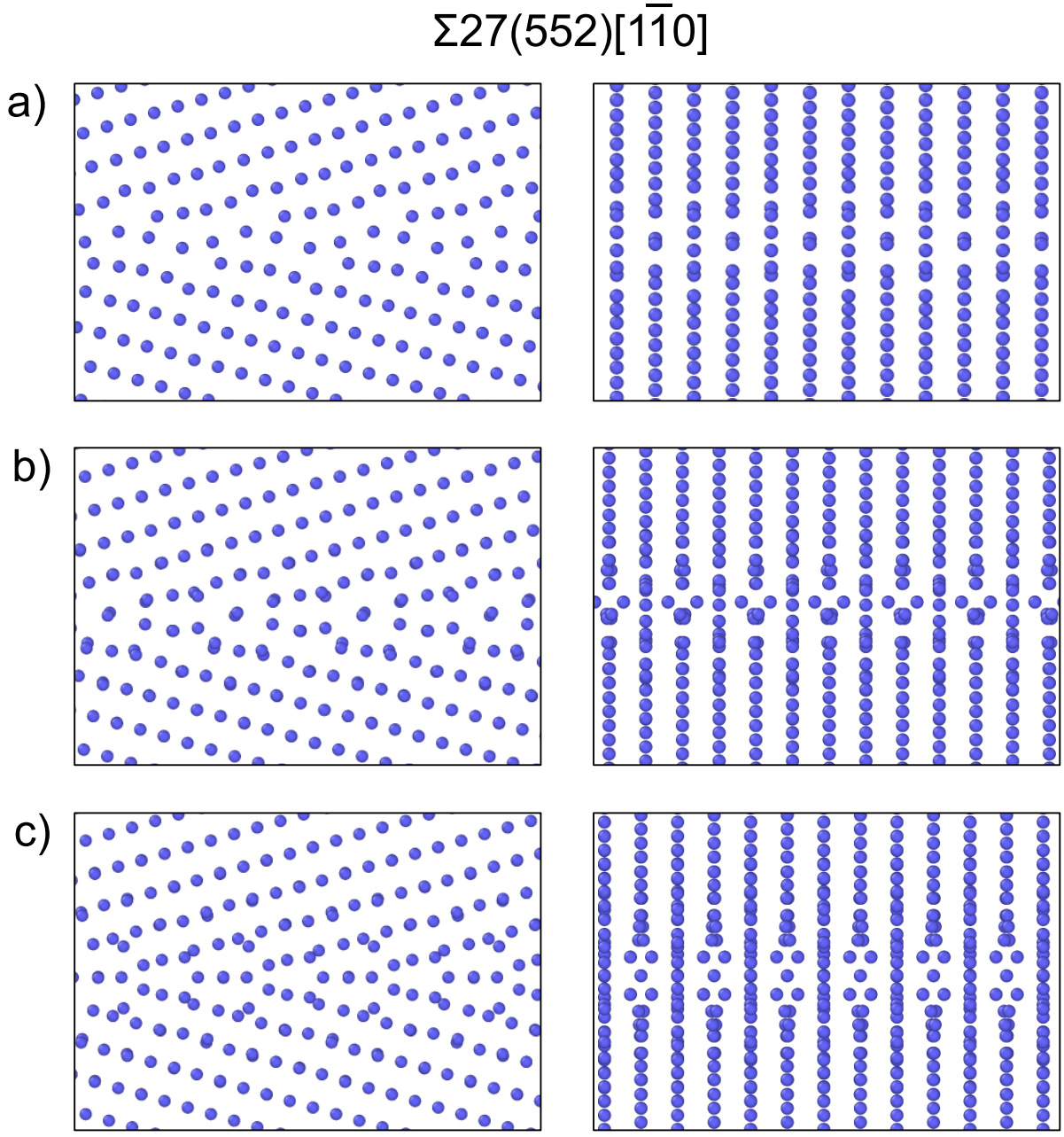

Figure 4: Multiple structures of $\Sigma27(552)[1\bar{1}0]$ grain boundary. a)Best configuration predicted by the traditional approach of γ-surface construction with GB energy $\gamma_{GB} = 2.67$ J/m^2 b) and c) Grain boundary structures obtained by GCS with atomic fractions 0 and 0.5 and energies $\gamma_{GB} = 2.495$ J/m^2 and $\gamma_{GB} = 2.493$ J/m^2, respectively. $\gamma_{GB} = 2.67$ J/m^2.

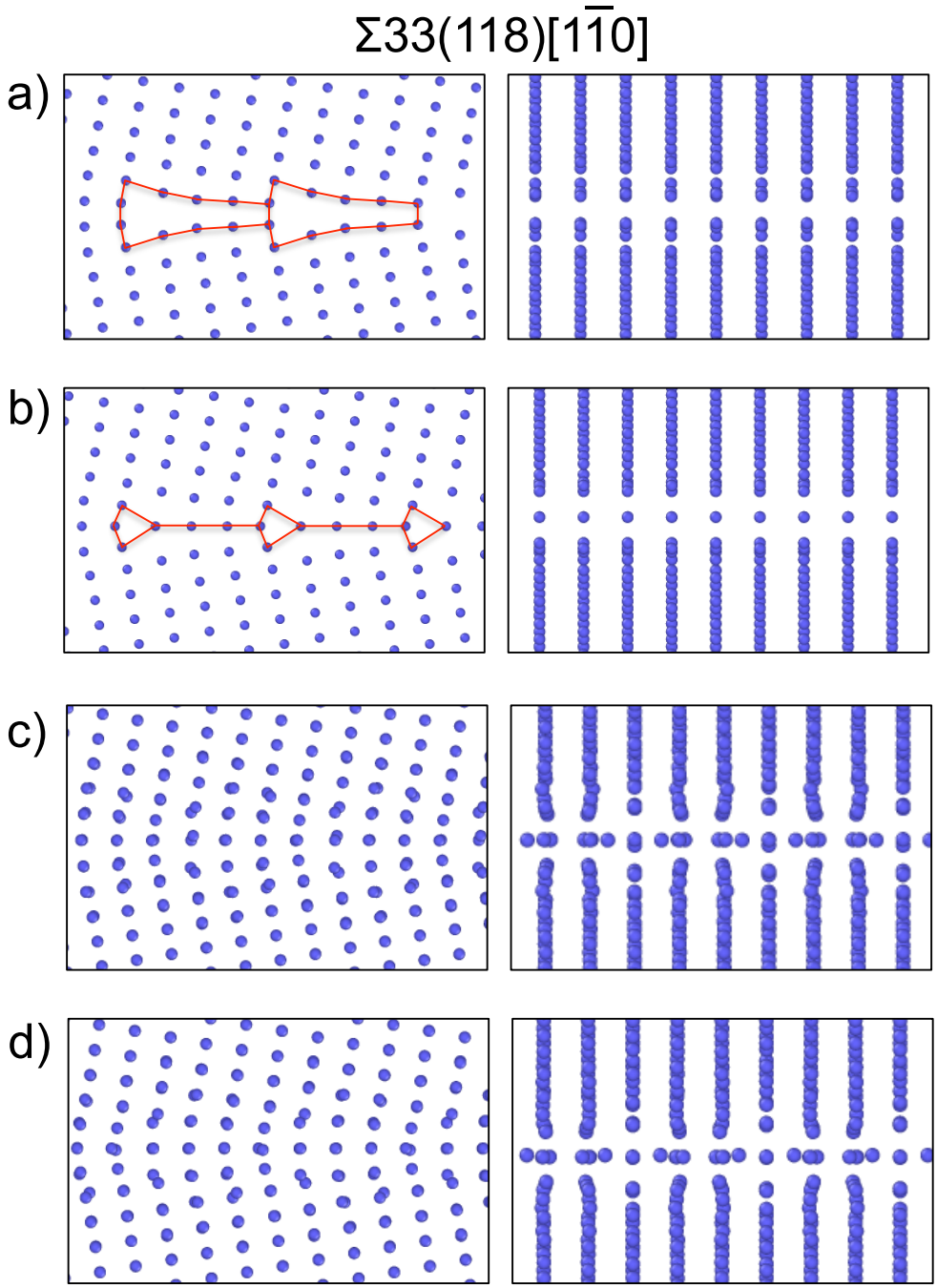

Figure 5: Structures of of $\Sigma 33(118)[1\bar{1}0]$ grain boundary (20.1°). a) Lowest energy state with $\gamma_{GB} = 2.611$ J/m^2 generated with the γ-surface approach using EAM1 potential, same structure as γ-surface approach with DFT[22, 21] b) γ surface approach with EAM2, $\gamma_{GB} = 2.257$ J/m^2 c) Grain boundary structures obtained by GCS using EAM1 with atomic fraction 0.333 and energy $\gamma_{GB} = 2.615$ J/m^2. d) Grain boundary structures obtained by GCS using EAM2 with the same atomic fraction of 0.333 and energy $\gamma_{GB} = 2.226$ J/m^2.

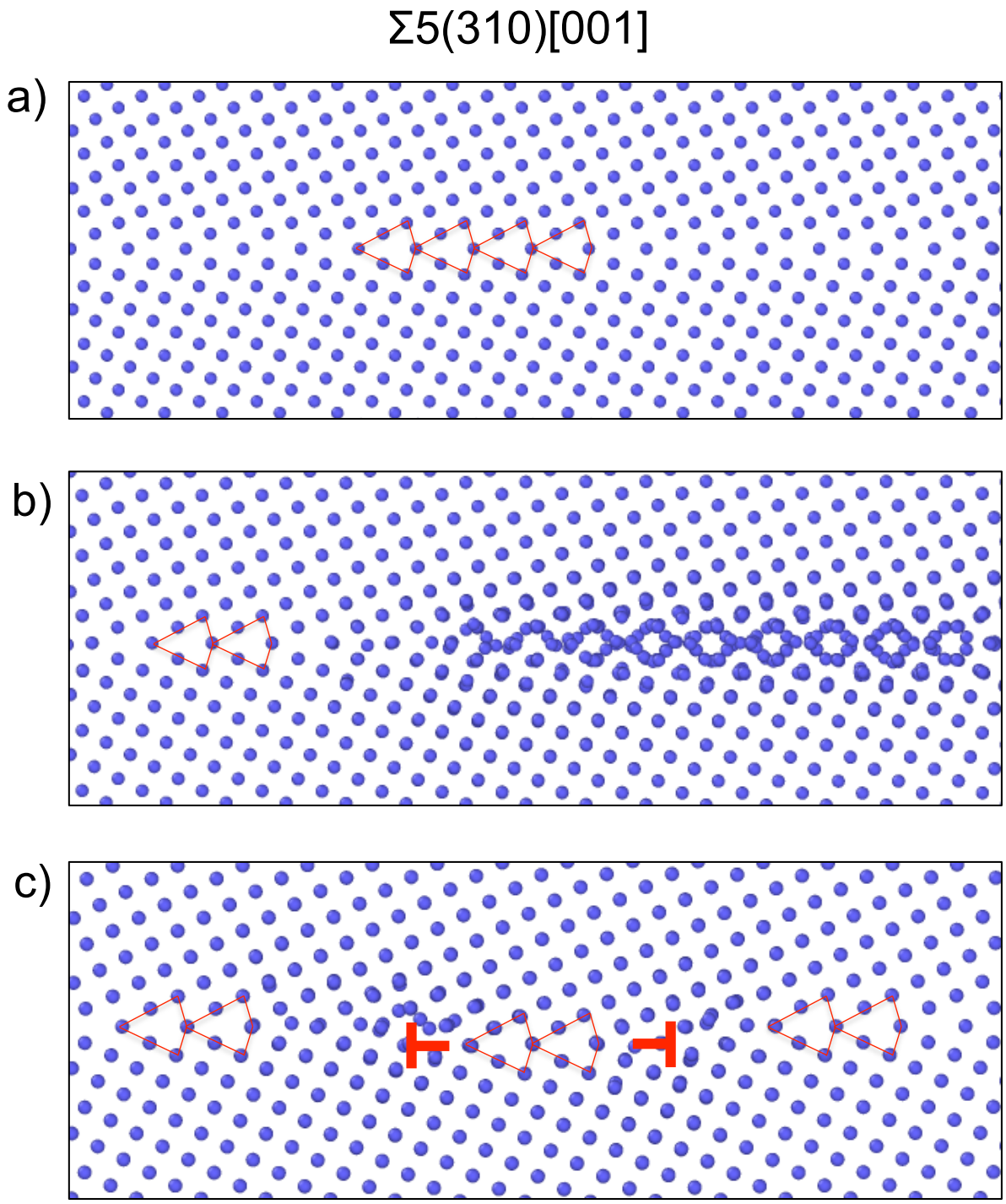

Figure 6: a)Interstitials are introduced into a bicrystal with perfect Σ5(310)[001] grain boundary. The grain boundary kite-shaped structural units are outlined in red. b) The atoms diffuse to the boundary and get absorbed by locally forming a metastable ordered grain boundary structure with higher energy. c) Metastable grain boundary segment transforms into an interstitial loop at the grain boundary.

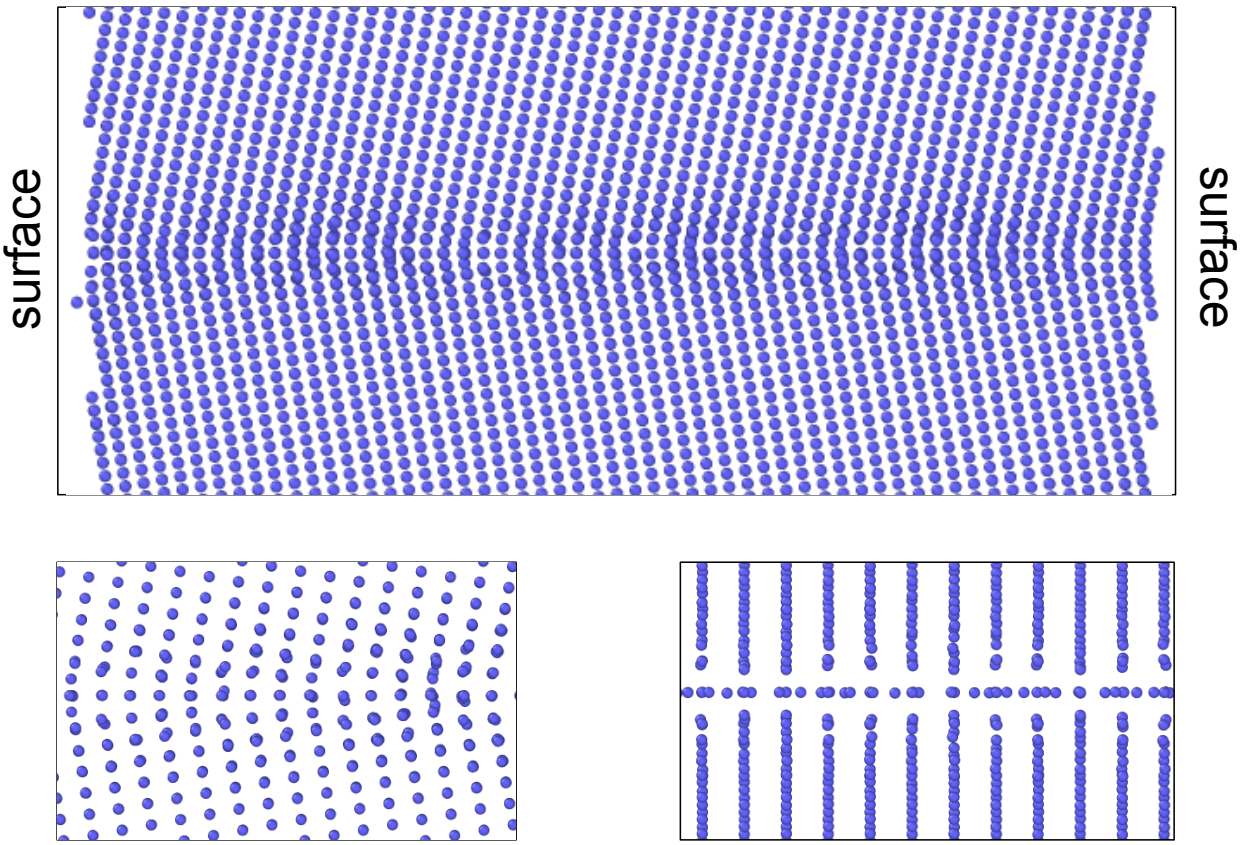

Figure 7: Validation and comparison of grain boundary structures found at 0K with grain boundary structures at finite temperature. Bicrystal with $\Sigma 33(118)[1\bar{1}0]$ grain boundary terminated at an open surface and annealed at 2500K for several nanoseconds. The open surface enables variation of atomic density. The high temperature GB structure is different from γ-surface constructed boundary, but matches the prediction of GCS calculations.

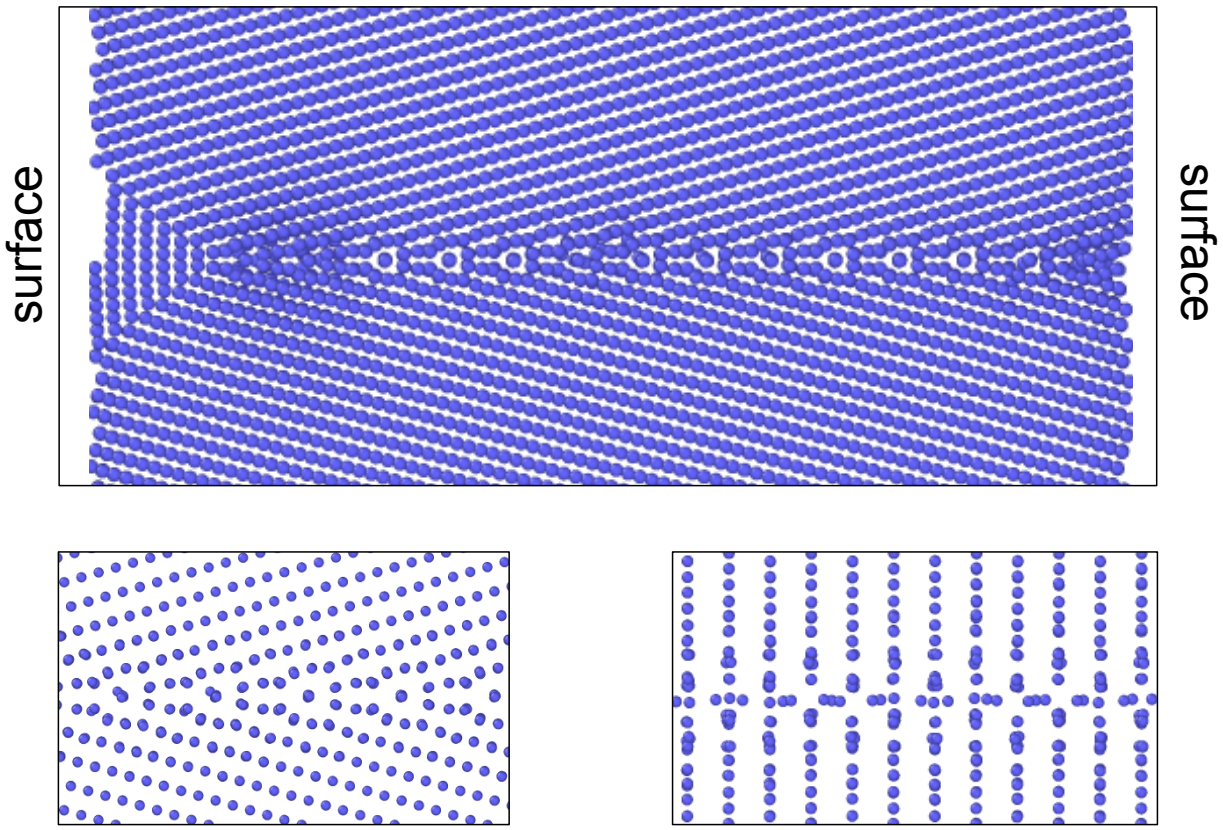

Figure 8: Validation and comparison of grain boundary structures found at 0K with grain boundary structures at finite temperature. Bicrystal with $\Sigma 27(552)[1\bar{1}0]$ grain boundary terminated at an open surface and annealed at 2500K for several nanoseconds. The open surface enables variation of atomic density. The high temperature GB structure is different from γ-surface constructed boundary, but matches the prediction of GCS calculations.